Characterization of HOCl Using Atmospheric Pressure Ionization Mass Spectrometry

Tracy E. Caldwell,† K. L. Foster, Thorsten Benter, Sarka Langer,‡ John C. Hemminger, and Barbara J. Finlayson-Pitts*

Department of Chemistry, University of California, Irvine, Irvine, California 92697-2025

Received: February 25, 1999; In Final Form: August 6, 1999

HOCl is an important intermediate in stratospheric and tropospheric chemistry. Although it can be readily measured in laboratory systems at low pressures (≤20 Torr) using conventional electron impact ionization mass spectrometry, there is a need for a measurement technique that can operate at higher pressures, up to 1 atm in air. One such technique seeing increasing use is atmospheric pressure ionization mass spectrometry (API-MS). We report here studies of the API-MS of ∼0.5−50 ppm HOCl at a total pressure of 1 atm and room temperature. Major peaks from the ion-adducts with Cl^- and OCl^- were observed. The Br^- adduct of HOCl can also be generated using bromoform in the discharge region of the ion source. At the lower range of HOCl concentrations studied in air, the O_2^- adduct and small parent peaks assigned to $HOCl^-$ were observed. The species present as minor impurities in the HOCl source (Cl_2, Cl_2O and HCl) can be readily distinguished through identification of the parent ion for Cl_2, or as their adducts with Cl^- and Br^- for Cl_2O and HCl. The identification of HOCl was confirmed using electron impact ionization time-of-flight mass spectrometry (EI-MS). HOCl was quantified using EI-MS to measure the Cl_2 generated when the HOCl reacted heterogeneously on a water−ice/HCl surface and independently by photolysis of the HOCl to generate atomic chlorine, which was trapped using propene and measured as chloroacetone. The implications for the use of API-MS for measuring HOCl in laboratory systems and in ambient air are discussed.

Introduction

The reactions of halogenated species have been of great interest with respect to stratospheric chemistry and ozone destruction processes.[1] HOCl, for example, is believed to be an important intermediate in the reaction of $ClONO_2$ with HCl on ice:[2]

$$ClONO_2 + H_2O \rightarrow HOCl + HNO_3 \quad (1)$$

$$HOCl + HCl/ice \rightarrow Cl_2 + H_2O \quad (2)$$

In laboratory studies of this reaction carried out under stratospheric conditions of low pressures (e.g., in fast flow systems), HOCl has been followed by conventional mass spectrometry with electron impact (EI) ionization using the strong parent peaks at $m/z = 52$, 54[3−8] and by chemical ionization mass spectrometry by reacting the HOCl with F^- ions to form ClO^-.[9] HOCl has been detected in the upper stratosphere by mass spectrometry as clusters with nitric and sulfuric acids and their anions, such as $NO_3^-(HNO_3)_nHOCl$ and $HSO_4^-(H_2SO_4)_mHOCl$, where $n = 1$, 2 and $m = 0$, 1 and $HSO_4^-(HNO_3)_2HOCl$.[10−12]

Recently, there has been increasing attention paid to the potential importance of inorganic halogen compounds formed in the reactions of sea salt in the troposphere.[13−15] One of these is HOCl, whose reactions with chloride and bromide in sea salt particles are predicted by modeling studies to lead to the formation of gaseous photochemically active Cl_2 and BrCl, respectively.[16,17] HOCl has not, however, yet been identified in the troposphere. Studies carried out under the conditions of the marine boundary layer require that sampling be carried out at atmospheric pressure with very high sensitivity toward the halogen species. While sampling into a conventional mass spectrometer, either pulsed or continuously, can be achieved using differential pumping, there is a concomitant loss of sensitivity. Hence, there is a need for accurate, specific, and sensitive methods of measurement of HOCl at atmospheric pressure.

A technique which has proven powerful for measuring certain species, such as dimethyl sulfide and the molecular halogens Cl_2 and Br_2 under tropospheric conditions, is atmospheric pressure ionization mass spectrometry (API-MS).[18] Because the use of atmospheric pressure in the ion source region precludes the use of hot filaments to generate the ionizing electrons, ionization is achieved through a corona discharge. Ionization of air in the high electric field region ($>10^6$ V m^{-1}) surrounding the corona discharge generates a series[19] of negative ions, including OH^-, O_2^-, NO_2^-, O_3^-, CO_3^-, HCO_3^-, NO_3^-, $OH{\cdot}CO_3^-$, and positive ions such as $H^+(H_2O)_n$. Depending on the electron and proton affinities of the trace species of interest, transfer of a proton or an electron to the trace gas of interest can occur, generating an ion which can be detected and measured. For example, using API-MS Spicer et al.[20] have recently reported measurements of Cl_2 in the marine boundary layer at concentrations up to ∼150 ppt at a coastal site. Electron transfer to Cl_2 generates parent peaks at $m/z = 70$, 72, and 74, and in the Spicer et al. study,[20] the MS/MS peaks unique to Cl_2 at $m/z = 70/35$, 72/35, 72/37, and 74/37 were measured.

Because of the complex ion−molecule chemistry in the

* To whom correspondence should be addressed; e-mail bjfinlay@uci.edu;phone (949) 824-7670; FAX (949) 824-3168.

† Current address: NASA Johnson Space Center, Mail Code CB, Houston, TX 77058.

‡ Current address: Department of Chemistry, Section for Inorganic Chemistry, University of Göteborg, S-412 96 Göteborg, Sweden; also at SP Swedish National Testing and Research Institute, Chemistry and Materials, Brinellgatan 4, Box 857, S-501 15 Borås, Sweden.

10.1021/jp9906841 CCC: $18.00
Published on Web 09/23/1999

source, other reactions leading to the formation of ions from the trace species of interest can also occur. This results in mass spectra which are more complex than those from electron impact ionization, especially when more than one trace analyte coexists in the mixture. As a result, the specificity and sensitivity of API-MS is highly dependent on the ion−molecule chemistry of air, as well as the trace components of the gas sample. We report here API-MS studies of HOCl in air at atmospheric pressure and, for comparison, EI-TOF mass spectra. The potential utility of this technique for following HOCl at atmospheric pressure in laboratory systems and in ambient air is discussed.

Experimental Section

1. Instrumentation. The API-MS (Perkin-Elmer Sciex, Model 300) consists of two mass filtering quadrupoles (Q1 & Q3) separated by a collision cell, which encloses a third quadrupole operating in the RF-only mode (Q2). Gas-phase samples are introduced at atmospheric pressure into the ion source region by a small, diaphragm pump-driven venturi system. This ion source region is separated from the high-vacuum mass analyzer stage by a 250-μm orifice. Reagent ions are produced in a corona discharge (up to 8 kV), the polarity of the point-to-plane field determining the polarity of the ions to be analyzed. All spectra reported here are taken in the negative ion mode. The ions generated in the ion source are drawn through a curtain of dry N_2 gas, which aids in declustering the primary ions as well as restricting sample and ambient air from entering the vacuum chamber. A potential gradient applied across the differentially pumped vacuum interface transfers ions from the source into the high vacuum mass analyzer region.

This instrument is capable of operating in two modes of acquisition: single MS mode (Q1 scan) or MS/MS mode (product scan). In single MS mode, the first quadrupole (Q1) is scanned through a range of masses to yield a conventional mass spectrum. These scans are useful for identifying ions based on their mass-to-charge ratio (m/z). In MS/MS mode, ions exiting the first quadrupole are collisionally dissociated using N_2 gas at a typical pressure of 8 mTorr. Quadrupoles Q1 and Q3 can also be operated as mass analyzers in some tandem combination specified by the operator. In the simplest of these scans, the *product scan*, the first mass filter (Q1) is held fixed at a particular m/z, allowing only those ions to pass. The ions selected using Q1 are fragmented in the collision cell and the resulting fragment ions pass through the final mass filter (Q3), producing a spectrum of the ion characteristic fragmentation pattern. Scans taken in the MS/MS mode are useful for elucidating the structure of the parent ions observed in the Q1 scan.

The electron impact ionization experiments were performed using a Bruker TOF1 time-of-flight mass spectrometer. The instrument is equipped with a two-stage gridless reflectron. With a total folded ion flight path length of 2 m and the time focusing properties of the reflectron, a mass resolution of $m/\Delta m \geq 800$ is achieved in the EI mode. The pulsed electron source was operated at a 20 Hz repetition rate with a duty cycle of 4.5 μs. All mass spectra were acquired using a standard electron energy of 70 eV and stored with 5 ns resolution in a LeCroy TR8828-based digitizer. The memory depth of this system enabled the acquisition of complete mass spectra in the range $m/z = 1-1000$. Typically 100 mass spectra were averaged before the selected mass regions of interest were integrated. For the quantitative measurements, the following mass signals were monitored simultaneously: $m/z = 54/52$ for HOCl, $m/z = 51/53$ for Cl_2O (see below), and $m/z = 70/72/74$ for Cl_2.

We have used a new pulsed inlet stage that enables operation of the MS at atmospheric pressure. This stage will be described in detail elsewhere, so only a brief outline is given here. The gated valve consists of a Teflon body equipped with inlet and outlet ports and a solenoid driven tappet. The solenoid is sealed from the sampling region by a Teflon diaphragm. All metal parts of the tappet are coated with an annealed Teflon film. This design allows for sampling at atmospheric pressure under slow flow conditions. Flow velocities of ≥ 0.5 m s^{-1} were used for the measurements described here. In separate experiments, it was shown that under these conditions HOCl samples do not decompose while residing in the sampling stage. The valve was differentially pumped with a 500 L s^{-1} turbo molecular pump. The total gas pulse length was measured to be ≤ 500 μs by following the signal intensity of a selected sample mass peak as a function of the delay time between the solenoid driver signal and the electron gun signal.

The HOCl calibration experiments were based on the rapid heterogeneous conversion of HOCl to Cl_2 on HCl/water ice surfaces (see below). A U-tube of 6 mm i.d. and a total length of 30 cm equipped with a bypass served as a heterogeneous reactor. The inlet port of this reactor was connected to a 30 L Teflon chamber containing HOCl in N_2 (Ultrahigh Purity, Oxygen Service Co., 99.999%) and the outlet port to the sampling stage of the TOF-MS. HCl/water ice surfaces were prepared by spraying a concentrated 37% aqueous HCl solution onto the precooled inner surface of the U-tube. The temperature of the tube was kept at 250 K using a liquid N_2-cooled acetone bath. Complete mass spectra were recorded continuously when the gas flow was switched from the bypass to the U-tube and vice versa.

A second approach to estimating the concentration of HOCl was also used. The stream of HOCl in the N_2 exiting the bubbler was diverted into a Teflon chamber containing approximately 10 L of a mixture of 123−147 ppm propene (Aldrich, >99%) in air to a total volume of 43 L. The mixture was photolyzed at 254 nm for 20 min using low-pressure mercury lamps (Jelight Co. Inc.), and the atomic chlorine generated by the HOCl photolysis[21] was trapped by reaction with propene, generating chloroacetone. The loss of propene and formation of chloroacetone were followed using GC-FID (Hewlett-Packard 5890 Series II) with a 30 m × 0.32 mm ID GS-Q column (J&W Scientific), which was held at 120 °C for 6 min, ramped at 25 °C min^{-1} to 220 °C, and then held at that temperature for 5 min. In independent runs in which the GC-FID was calibrated for chloroacetone (Acros, 96%, stabilized with 0.5% $CaCO_3$) and propene, the yield of chloroacetone from the chlorine atom−propene reaction under these conditions was determined to be $63 \pm 4\%$ (2σ). The loss of chloroacetone by photolysis at 254 nm for 20 min, as in the HOCl photolysis, was measured in separate runs to be $16 \pm 4\%$ (2σ).

2. Reagents. HOCl was prepared in solution by the slow, dropwise addition of 250 mL of NaOCl (Aldrich, 13% available chlorine) into a slurry of 40 g of anhydrous $MgSO_4$ (Fisher Scientific, reagent grade) and 200 mL of Nanopure water (Barnstead, $\rho > 18$ MΩ) while constantly stirred.[22] The solution turns an opaque-peach color, forming a precipitate which is not separated prior to the low-vacuum distillation (35 Torr). The temperature of the reaction flask is increased from 25 to 45 °C through the course of the distillation (2.5 h), and the HOCl solution is collected in a receiving flask cooled to −20 °C. This method provides a relatively safe, simple, and stable source of HOCl and hence is preferred over the more standard synthesis involving hydrolysis of the explosive Cl_2O.

Gas-phase HOCl was generated by bubbling either N_2 or air (Scott-Marrin Ultrapure; manufacturer's specifications are total hydrocarbons as $[CH_4] < 0.01$ ppm, $[CO] < 0.01$ ppm, $[NO_x] < 0.001$ ppm, and $[SO_2] < 0.001$ ppm) through a freshly prepared solution at room temperature, generating gaseous HOCl in the presence of water vapor. Cl_2 impurities originating from the slow decomposition of HOCl in the aqueous solution are minimized by bubbling for a few minutes prior to use. HCl and Cl_2O impurities are well below 1%, as determined by EI-TOF-MS.

DOCl was prepared by passing Cl_2O gas through a trap of liquid D_2O (Cambridge Isotope Laboratories, Inc., 99.9%). This method yields a very small amount of DOCl and, as a consequence, is observed only by flowing directly into the API-MS, by-passing the Teflon analysis chamber. Cl_2O was synthesized by passing a low flow of Cl_2 (Matheson, 1% in He), dried by passing through a trap of concentrated sulfuric acid, through a U-tube filled with yellow HgO (Aldrich, 99+%). Prior to use, the HgO is washed in 5 M NaOH, rinsed in Nanopure water, and dried (with stirring) at 125−130 °C for 10 h. The HgO is mixed with crushed glass to increase the surface area for reaction with Cl_2. The Cl_2O was flowed directly into the Teflon chamber for subsequent analysis with API-MS.

$CHBr_3$ (Aldrich, 96%) and $CHCl_3$ (Fisher Scientific, ACS certified), used for chemical ionization; HCl (Fisher Scientific, 37% in water), for quantification by conversion of the HOCl to Cl_2; as well as Cl_2 (Matheson, 99.5%) and HCl (Scott Specialty Gases, 99.995%) gases, for calibration, are used without any further purification.

Results and Discussion

1. API-MS of HOCl. Figure 1 shows the Q1 (single MS) scan in the negative ion mode of air as well as HOCl at ∼1 and 50 ppm in air (note that these are approximate concentrations, since they were not actually measured in these particular runs; see section on quantification below). In the air spectrum (Figure 1a), peaks at m/z = 32, 46, 48, 60, 61, 62, and 77 are observed. These have been assigned by other researchers[19] to O_2^-, NO_2^-, O_3^-, CO_3^-, HCO_3^-, NO_3^-, and $CO_3^-\cdot$OH respectively formed from well-known ion−molecule reactions in the corona discharge.

Upon addition of HOCl (Figure 1b,c), a series of prominent new peaks are observed and are assigned as follows: Cl^- (m/z = 35, 37), ClO^- (m/z = 51, 53), $Cl^-\cdot$HOCl (m/z = 87, 89, 91), $Cl^-\cdot CO_3$ (m/z = 95, 97), $NO_3^-\cdot$Cl (m/z = 97, 99), and $ClO^-\cdot$HOCl (m/z = 103, 105, 107). At the lower HOCl concentration (Figure 1b), small peaks at m/z = 52, 54, corresponding to parent peaks of HOCl, are observed, as well as peaks at m/z = 84, 86, assigned to the adduct $O_2^-\cdot$HOCl. In addition, there are smaller peaks in Figure 1b,c which can be assigned to Cl_2^- (m/z = 70, 72, 74) and $Cl^-\cdot$HCl (m/z = 71, 73, 75) from very small amounts of Cl_2 and HCl impurities respectively (see below). There are also small peaks due to $ClO^-\cdot$(2HOCl) (m/z = 155, 157, 159, 161) and $Cl^-\cdot$(2HOCl) (m/z = 139, 141, 143, 145). As increasing concentrations of HOCl are sampled, the peaks in air from O_2^-, O_3^-, CO_3^-, HCO_3^- and $CO_3^-\cdot$OH decrease, and the intensities of the $ClO^-\cdot$HOCl peaks increase relative to those from $Cl^-\cdot$HOCl.

Table 1 summarizes the major fragments observed by MS/MS for each of the parent ions. The assignments given above are consistent with the MS/MS of each ion, as well as with the relative peak heights within a group, which are representative

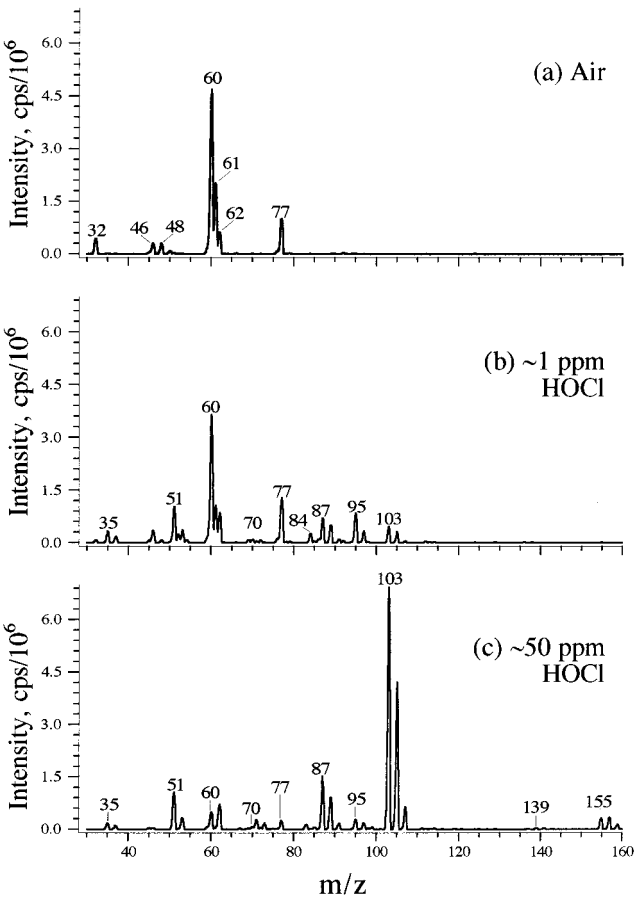

Figure 1. Mass spectrum (Q1 scan) of (a) air and gas-phase HOCl at (b) ∼1 ppm and (c) ∼50 ppm. The air peaks have not been subtracted from the HOCl spectra, so ions from ambient air also appear at m/z = 32 (O_2^-), 46 (NO_2^-), 48 (O_3^-), 60 (CO_3^-), 61 (HCO_3), 62 (NO_3^-), and 77 ($CO_3^-\cdot$OH). The gas stream exiting the flask containing HOCl was diluted in a flow system using air prior to entering the API-MS instrument.

of the naturally occurring abundance of the ^{35}Cl and ^{37}Cl isotopes. For example, ions such as ClO^- and $O_2^-\cdot$HOCl containing only one chlorine have relative isotopic abundances of ^{35}Cl:^{37}Cl = 3:1. Those containing two chlorines such as $Cl^-\cdot$HOCl and $ClO^-\cdot$HOCl have three isotopic peaks corresponding to the combinations $^{35}Cl^{35}Cl$, $^{35}Cl^{37}Cl$, and $^{37}Cl^{37}Cl$ respectively, in the relative ratios 9:6:1. Finally, the dimer adduct peaks such as $ClO^-\cdot$(2HOCl) which contain three chlorines, have four peaks corresponding to the combinations $^{35}Cl^{35}Cl^{35}Cl$, $^{35}Cl^{35}Cl^{37}Cl$, $^{35}Cl^{37}Cl^{37}Cl$, and $^{37}Cl^{37}Cl^{37}Cl$, with relative peak intensities of 27:27:9:1.

In some runs, N_2 was used as the carrier gas for the HOCl and the gas stream was flowed into a 30 L Teflon reaction chamber. Because the Teflon chamber and ion source region are not vacuum tight, there was also some air present during the ionization of these samples. The gas stream was also saturated with water vapor, which provides an additional source of oxygen and hydrogen in the discharge. The mass spectra were very similar to those in Figure 1b,c, except that the O_2^- adducts and small parent peaks of HOCl were not observed. Potential reasons for this are discussed below.

The identification of the Cl^- and ClO^- adducts with HOCl was further confirmed by examining the API-MS of DOCl. Figure 2 compares the API-MS Q1 scan of (a) HOCl formed using the $NaOCl/MgSO_4$ synthesis and (b) DOCl using the reaction of Cl_2O with D_2O in the region m/z = 85−110. The spectrum in Figure 2b shows peaks which are shifted by 1 amu,

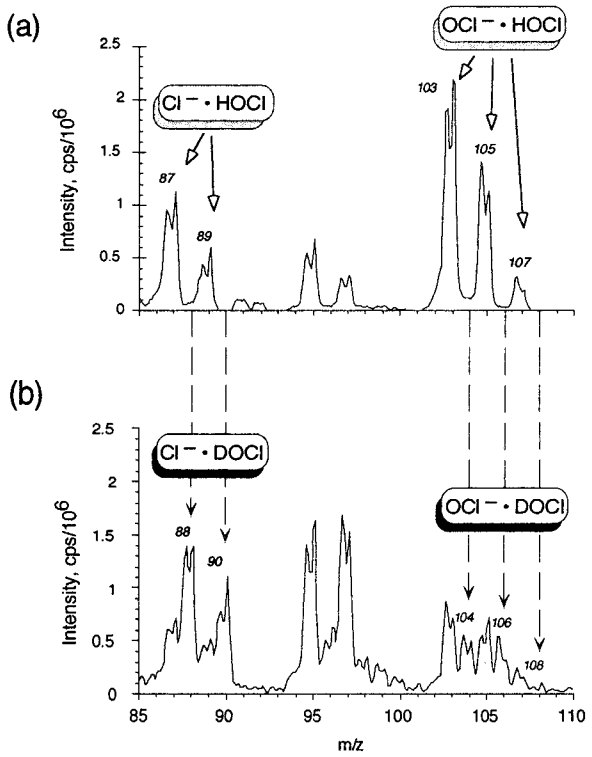

Figure 2. (a) Q1 scan of HOCl (~4 ppm) in N_2 with arrows indicating the observed adduct peaks; (b) Q1 scan of DOCl (and some HOCl) with dashed arrows indicating the deuterated peaks, which are shifted by one mass unit relative to their analogous HOCl peaks. The splitting of the peaks is due to nonoptimized tuning of the ion optics.

TABLE 1: Major Peaks Observed in API-MS of HOCl and Major Fragments from Their Collisional Dissociation

parent ion		major fragments	assignment
m/z	assignment	in MS-MS mode	of fragments
84	$HO^{35}Cl \cdot O_2^-$	32	O_2^-
		35	$^{35}Cl^-$
		51	$^{35}ClO^-$
86	$HO^{37}Cl \cdot O_2^-$	32	O_2^-
		37	$^{37}Cl^-$
		53	$^{37}ClO^-$
87	$Cl^- \cdot HOCl$ (both ^{35}Cl)	35	$^{35}Cl^-$
89	$Cl^- \cdot HOCl$ (one ^{35}Cl, one ^{37}Cl)	35, 37	$^{35,37}Cl^-$
91	$Cl^- \cdot HOCl$ (both ^{37}Cl)	37	$^{37}Cl^-$
103	$ClO^- \cdot HOCl$ (both ^{35}Cl)	35	$^{35}Cl^-$
		51	$^{35}ClO^-$
105	$ClO^- \cdot HOCl$ (one^{35}Cl, one^{37}Cl)	35, 37	$^{35,37}Cl^-$
		51, 53	$^{35,37}ClO^-$
107	$ClO^- \cdot HOCl$ (both ^{37}Cl)	37	$^{37}Cl^-$
		53	$^{37}ClO^-$
155	$ClO^- \cdot (2HOCl)$ (all ^{35}Cl)	103	$^{35}ClO^- \cdot HO^{35}Cl$
157	$ClO^- \cdot (2HOCl)$ (two ^{35}Cl, one ^{37}Cl)	103	$^{35}ClO^- \cdot HO^{35}Cl$
		105	$^{37}ClO^- \cdot HO^{35}Cl$, $^{35}ClO^- \cdot HO^{37}Cl$
159	$ClO^- \cdot (2HOCl)$ (one ^{35}Cl, two ^{37}Cl)	105	$^{37}ClO^- \cdot HO^{35}Cl$, $^{35}ClO^- \cdot HO^{37}Cl$
		107	$^{37}ClO^- \cdot HO^{37}Cl$
161	$ClO^- \cdot (2HOCl)$ (all ^{37}Cl)	107	$^{37}ClO^- \cdot HO^{37}Cl$

as expected for the $Cl^- \cdot DOCl$ and $OCl^- \cdot DOCl$ adducts. In addition, the MS/MS of the DOCl peaks are identical to those obtained for the analogous HOCl peaks.

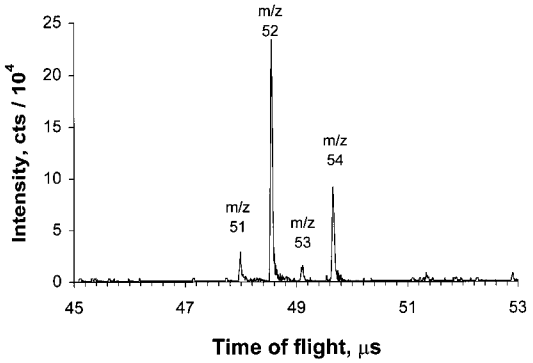

Figure 3. 70 eV electron impact time-of-flight raw mass spectrum of HOCl obtained from the Teflon analysis chamber. The base peak is the parent ion signal at $m/z = 52$ ($HO^{35}Cl^+$). The signals at $m/z = 51$, 53 ($^{35/37}ClO^+$) are due to ionic fragmentation of HOCl and to a minor extent from Cl_2O (see text). The Cl_2O concentration calculated from the ClO^+ fragment intensities is ≤1%.

For comparison, Figure 3 shows a 70 eV EI mass spectrum of HOCl; strong parent peaks (positive ion) at $m/z = 52$, 54 are evident, which is the basis of the detection and measurement of HOCl in laboratory systems at low pressures. However, in API-MS in the negative ion mode, fragments and clusters of HOCl predominate. This suggests that the initial steps in the atmospheric pressure ionization of HOCl in air do not involve primarily simple electron transfer, but rather, more complicated processes involving deprotonation and/or decomposition of HOCl.

This is reasonable based on the relatively small electron affinity of HOCl, calculated[23] to be 0.27 eV, relative to those of O_2^- (0.44 eV), O_3^- (2.1 eV) and CO_3^- (2.7 eV).[24,25] It is possible that direct electron attachment to HOCl results primarily in the following dissociation

$$e^- + HOCl \rightarrow Cl^- + OH \quad (3)$$

given that a similar attachment reaction for HNO_3

$$e^- + HNO_3 \rightarrow NO_2^- + OH \quad (4)$$

is found to be quite fast, $k_4 = (5 \pm 3) \times 10^{-8}$ cm^3 molecule^{-1} s^{-1}, with $\Delta H = -7$ kcal mol^{-1}.[26] Fehsenfeld et al.[26] suggest that, if very little rearrangement of bond angles and distances is required going from HNO_3 to (NO_2^- + OH), then the attachment process would be nearly vertical, favoring a rapid electron attachment process. The same may be true of HOCl, since the OH bond distance in HOCl is 0.975 ± 0.003 Å,[27] very close to the equilibrium internuclear separation of gas-phase OH (0.9706 Å).[28]

Reaction 3 is one source of Cl^- for the $Cl^- \cdot HOCl$ adducts observed in Figure 1. Other potential sources of Cl^- include the reactions of OH^- (see below) in the discharge region with small amounts of Cl_2 and HCl present as impurities. Dissociative ionization of Cl_2 in the discharge is less likely since the Q1 mass spectrum of Cl_2 alone indicates very little dissociation to Cl^-, even at concentrations >10 ppm. The signal for Cl^- increases by an order of magnitude relative to the Cl_2^- signal when HOCl, with the accompanying water, is present.

The peaks assigned to O_2^-, O_3^-, CO_3^-, HCO_3^-, and $CO_3^- \cdot OH$ peaks in air decrease when HOCl (with the accompanying water vapor) is added. However, when only water vapor is present in the air stream, the O_3^- peak increases; there is no significant change in the O_2^- or HCO_3^- peaks and those due to CO_3^- and $CO_3^- \cdot OH$ decrease. The addition of water

vapor to the corona discharge is known to increase the production of OH^- through reactions such as[29]

$$H_2O + e^- \rightarrow H^- + OH \quad (5)$$

$$H^- + H_2O \rightarrow OH^- + H_2 \quad (6)$$

The observed increase in O_3^- in the presence of water vapor is therefore consistent with a contribution to its formation by the fast electron transfer from OH^-, which has a smaller electron affinity (1.8 eV compared to 2.1 eV for O_3):

$$OH^- + O_3 \rightarrow O_3^- + OH \quad (7)$$

The decrease in CO_3^- and $OH{\cdot}CO_3^-$ can be attributed to effects of hydration of O_3^- on its switching reaction with CO_2:

$$O_3^- + CO_2 \rightarrow CO_3^- + O_2 \quad (8)$$

This reaction occurs[30] with a rate constant of 5.5×10^{-10} cm^3 $molecule^{-1}$ s^{-1} for O_3^-, but if two waters of hydration are attached to O_3^-, the rate constant falls to $<1 \times 10^{-10}$ cm^3 $molecule^{-1}$ s^{-1}.

The presence of HOCl in addition to water would be expected to remove OH^- by an acid−base reaction, generating OCl^- simultaneously:

$$OH^- + HOCl \rightarrow H_2O + OCl^- \quad (9)$$

The HOCl dimer may undergo similar reactions. An acid−base reaction of HOCl with HCO_3^- would be expected as well. Such reactions are the likely source of OCl^- for formation of the observed OCl^- adducts. Since OH^- reactions in the absence of HOCl generate other species such as O_3^-, competition from its removal via acid−base reactions such as (9) would be expected to lead to decreases in these "air peaks", consistent with our observations. This is also supported by the measured effects of addition of HCl, which changes the O_2^-, O_3^-, CO_3^-, HCO_3^-, and $CO_3^-{\cdot}OH$ peaks in a manner similar to that of HOCl; the simultaneous decrease in the O_2^- peak in this case is consistent with HCl being a stronger acid than HO_2, so that proton transfer occurs from HCl to O_2^- (but as discussed below, not from HOCl).

It is common to form relatively strong association complexes between ions and neutrals. Reaction rate constants and equilibrium constants for a number of three-body association reactions between negative ions and neutral molecules have been measured using flowing afterglow systems.[26,30−33] For example, the termolecular rate constant of formation for $NO_3^-{\cdot}HNO_3$, similar to $OCl^-{\cdot}HOCl$ observed here, is $>1 \times 10^{-26}$ cm^6 $molecule^{-2}$ s^{-1}, with lifetimes of the adduct on the order of 10^{-9} s at room temperature.[26] Theoretical studies focusing on ion−neutral attachment support the experimental evidence, with association energies typically over 20 kcal mol^{-1} exothermic for these reactions.[34,35] Indeed, ab initio calculations of $Cl^-{\cdot}HOCl$ predict the binding energy of this complex to be 23.4 ± 2 kcal mol^{-1}, where the minimum energy conformation corresponds to the chloride ion complexing with the hydrogen of HOCl.[35] The formation of adducts of HOCl dimers with Cl^- and ClO^- observed here also has an analogy with HNO_3.[26] In this case, the dimer complexes were proposed to be formed by the rapid replacement of water in $NO_3^-{\cdot}HNO_3{\cdot}H_2O$:

$$NO_3^-{\cdot}HNO_3{\cdot}H_2O + HNO_3 \rightarrow NO_3^-{\cdot}2HNO_3 + H_2O \quad (10)$$

TABLE 2: Gas-Phase Acidities of Some Acids

heterolytic reaction	$\Delta H_{acid}(AH)$[a] (kJ mol^{-1})
$HF \rightarrow F^- + H^+$	1554 ± 1
$HOCl \rightarrow OCl^- + H^+$	1502 ± 9
$HO_2 \rightarrow O_2^- + H^+$	1476 ± 9
$HCl \rightarrow Cl^- + H^+$	1395 ± 1
$HNO_3 \rightarrow NO_3^- + H^+$	1358 ± 1
$HBr \rightarrow Br^- + H^+$	1354
$HI \rightarrow I^- + H^+$	1315

[a] From ref 25.

Adducts of HOCl with NO_3^- and HSO_4^- have also been observed in the upper stratosphere.[10−12]

Adducts of HOCl with Cl^- and O_2^- are consistent with the relative gas-phase acidities of HOCl, HCl, and HO_2. The gas-phase acidity of an acid, HA,

$$HA \rightarrow H^+ + A^- \qquad \Delta H_{acid}(AH) \quad (11)$$

increases as the dissociation energy, $\Delta H_{acid}(AH)$, decreases.[36] The dissociation energies in Table 2[25] show that gas-phase acid strength follows the trend HI > HBr > HNO_3 > HCl > HO_2 > HOCl > HF. One would therefore expect gas-phase HOCl deprotonation when F^- is present, which has been reported,[9] though not in the case of O_2^- or any of the other halide ions (Cl^-, Br^-, or I^-). This is consistent with the report that I^- does not deprotonate HOCl to OCl^-.[37] Evidence of this trend is also observed for HNO_3, where reaction with ions to the right in this trend lead to exothermic processes and those to left are endothermic.[26] As shown here, those conjugate anions of acids having higher gas-phase acidities (such as Cl^- and O_2^-, and as discussed below, Br^-) undergo adduct formation with HOCl rather than deprotonation of the HOCl.

There are several potential sources for the small parent peaks at $m/z = 52, 54$. One possibility is electron transfer from a species with a small electron affinity, for example from O_2^- in competition with adduct formation. Another possibility is a minor second channel in reaction 3, generating $HOCl^-$, which is stabilized at the atmospheric pressure.

Impurities expected to be present in the HOCl include Cl_2 (for which small peaks at $m/z = 70, 72, 74$ are observed in Figure 1), HCl, and Cl_2O from the equilibrium in eq 12

$$Cl_2O + H_2O \leftrightarrow 2\ HOCl \quad (12)$$

However, they are present at much smaller concentrations and are easily differentiated from HOCl. For example, the Q1 mass spectrum due to Cl_2O is shown in Figure 4. It was obtained from an HOCl solution which was stored in the dark at temperatures below the freezing point of water ice. Due to the equilibrium between HOCl and Cl_2O, some Cl_2O exists in solution. The solution was used when still below room temperature, which shifts the equilibrium toward Cl_2O production. Cl_2O is readily discernible in Figure 4 as Cl^- and OCl^- adducts ($Cl^-{\cdot}Cl_2O$ and $OCl^-{\cdot}Cl_2O$), with relative peak intensities of 27:27:9:1, as expected. These Cl_2O adduct peaks are absent from spectra taken immediately following the HOCl synthesis with the liquid sample held at room temperature. The EI mass spectrum in Figure 3 is also evidence that Cl_2O was not a significant impurity in the HOCl. Cl_2O has strong fragment peaks at $m/z = 51, 53$. However, the large relative peak intensities for $m/z = 52, 54$ compared to the 51, 53 peaks is characteristic of HOCl, with an upper limit to the contribution from Cl_2O of <1%.

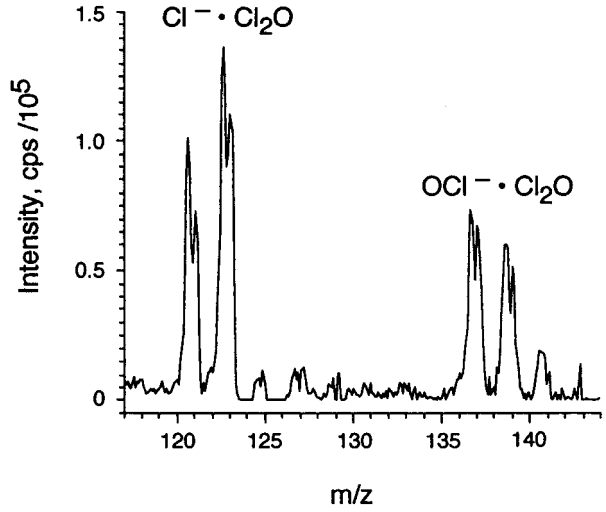

Figure 4. Q1 scan obtained from a "cold" HOCl solution using N_2 as the carrier gas. Background noise and peaks (e.g. at $m/z = 123$) have not been subtracted out. With background subtraction, these peaks (both $Cl^- \cdot Cl_2O$ and $OCl^- \cdot Cl_2O$) exhibit relative intensities of 27:27:9:1. The splitting of the peaks is due to nonoptimized tuning of the ion optics.

Mass spectra of Cl_2O were obtained for comparison by reacting Cl_2 gas with solid HgO. It is impossible, however, to eliminate the presence of water in the sampling system and API source which reacts with Cl_2O to form HOCl; therefore, the spectrum of Cl_2O from this synthesis looks almost identical to that in Figure 4 from the HOCl synthesis.

Although the electron affinity[24,25] of Cl_2O (2.2 eV) is higher than that of O_2 (0.44 eV) and O (1.46 eV), Cl_2O does not undergo simple charge transfer with these ion species in the corona discharge, as evidenced by the lack of Cl_2O parent peaks at m/z 86, 88, and 90. The adduct peaks are the only unambiguous indicators of the presence of Cl_2O.

HCl is likely to be only a minor impurity because it is rapidly removed in the HOCl solution:

$$HOCl_{(l)} + HCl_{(l)} \rightarrow Cl_{2(g,l)} + H_2O_{(l)} \qquad (13)$$

The major peaks observed for HCl in air alone are at $m/z = 35$ and 37, as well as at $m/z = 68$ and 70 ($O_2^- \cdot HCl$) with slightly lower intensity. HCl in the presence of other chlorine sources (HOCl and $CHCl_3$), though, is more predominantly recognized as the $Cl^- \cdot HCl$ adducts at $m/z = 71$, 73, and 75. In the spectrum of pure HCl (in air or in the presence of other chlorine sources), no signal is observed at those masses which have been attributed to either HOCl or Cl_2O. On the basis of experience with this synthesis of HOCl in previous studies,[21] HCl is present at levels <1%.

2. Quantification of HOCl. Two methods were used to determine the concentration of HOCl. The first is based on the heterogeneous reaction (13), where gas-phase HOCl reacts with condensed phase HCl present in excess in an water−ice matrix. A reaction probability of >0.3[9] has been calculated on the basis of results from flow tube studies. EI-MS was employed to quantify the Cl_2 formed in this reaction and thus to measure quantitatively the HOCl concentration. The integrated ion signals for both $HO^{37}Cl$ ($m/z = 54$) and $^{37}Cl_2$ ($m/z = 74$), recorded simultaneously, are shown in Figure 5. Upon switching the gas flow from the bypass to the U-tube, signals at $m/z = 51-54$ disappear quantitatively within the time scale of two integration steps, i.e., 10 s. At the same time, rapid production of Cl_2 is observed. When the flow is switched back, the recovery time of the HOCl signal is roughly a factor of 10−20 longer, with Cl_2 signals showing similar, but uncorrelated, behavior. We attribute these slower recoveries to the heterogeneous reaction of HOCl with small amounts of HCl/H_2O that have been swept out of the U-tube into the Teflon sampling line upon switching the gas flow.

Blank runs with HOCl flowing through an empty U-tube held at 250 K revealed a relative increase of ClO^+ fragment ion signals at $m/z = 51/53$. Under these conditions the equilibrium (12) is shifted to the left, resulting in additional formation of Cl_2O. In 70 eV electron impact mass spectra, Cl_2O has a weak parent ion peak at $m/z = 86$ (as well as 88 and 90) but strong ionic fragment signals at $m/z = 51/53$. It has not been determined whether the reaction of HOCl with HCl is fast enough to suppress Cl_2O formation on the cold surface via reaction (12) or whether any Cl_2O formed is directly converted [possibly after hydrolysis (12)] into Cl_2:

$$Cl_2O(g) + 2HCl \rightarrow 2Cl_2(g) + H_2O \qquad (14)$$

However, since signals due to both HOCl *and* Cl_2O disappear upon exposure of the sample gas flow to the HCl/water−ice surface, the concentration of heterogeneously generated Cl_2 reflects the total concentration of HOCl in the room-temperature gas flow. We were not able to detect any ion signals due to HOCl, Cl_2O, or Cl_2 when the U-tube was warmed to room temperature after the run, indicating quantitative release of Cl_2. In addition, air passing through the HCl/ice-coated U-tube in the absence of HOCl produced no detectable Cl_2. The increase in the calibrated Cl_2 signal due to the heterogeneous reaction is $(2.4 \pm 0.3) \times 10^{15}$ molecule cm^{-3}, corresponding to an HOCl concentration of 98 ± 12 (2σ) ppm.

The second method of quantification of HOCl yielded similar results. Two runs were carried out in which 85−90% of the HOCl was photolyzed in the presence of propene to generate chlorine atoms, which were trapped by reaction with the C_3H_6 to form chloroacetone. The loss of HOCl due to photolysis was measured using API-MS in the MS/MS mode. On the basis of our measured yield (63%) of chloroacetone in the $Cl + C_3H_6$ reaction under these conditions and after correction for loss of chloroacetone by photolysis (16%), the concentration of HOCl in the gas stream diverted into the Teflon chamber containing the propene was estimated to be 36 ± 7 (2σ) ppm. In these studies, however, the $HOCl/N_2$ passed through a flowmeter between the bubbler and Teflon chamber, and this was found in subsequent studies to decompose significant amounts of HOCl. Correcting for the loss through the flowmeter, measured independently using API-MS, the concentration of HOCl in the N_2 stream exiting the bubbler was estimated to be 102 ± 21 ppm (2σ; the error reflects those in chloroacetone measurements only so that the true error, which includes variability in the flowmeter losses, is larger), in excellent agreement with the EI-MS measurements.

3. Application of API-MS to Atmospheric Measurements of HOCl. Because HOCl does not have a strong parent peak in API-MS, ion adducts are likely to be most useful in its detection and measurement in the atmosphere. One possibility is the O_2^- adduct at $m/z = 84$, 86. Another is the creation of new adducts such as those of the bromide ion generated in the corona disharge through the addition of organobromine compounds to the airstream. This has the advantage that an additional isotopic signature due to bromine is found in the adduct, providing further specificity to the measurement.

For example, Figure 6 compares the API-MS for HOCl using ambient air or $CHBr_3$, respectively, in the ion source. The

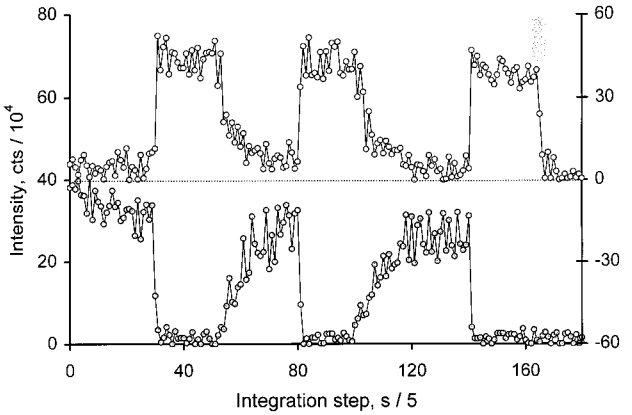

Figure 5. Integrated mass signals of $HO^{37}Cl$, lower trace ($m/z = 54$), and $^{37}Cl_2$, upper trace ($m/z = 74$), simultaneously recorded in a heterogeneous titration experiment. Each data point represents the integrated peak area of a selected m/z region in the TOF spectrum after 100 mass spectra have been acquired. At the time indicated by the arrow, the HOCl flow was stopped and N_2 was flowed through the U-tube.

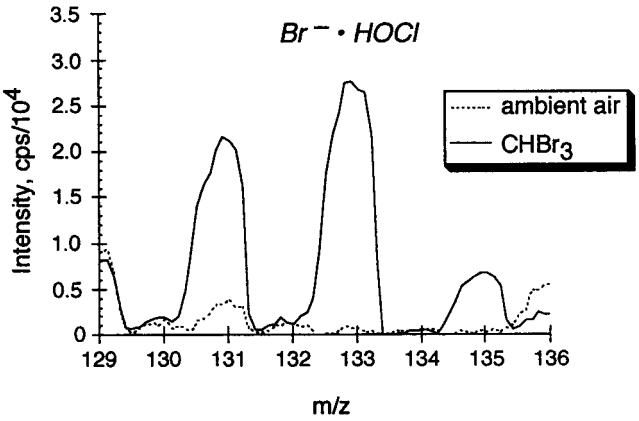

Figure 6. Q1 scan of 100 ppm HOCl upon the addition of bromoform to the ion source region. Peaks at $m/z = 131$, 133, and 135 correspond to the formation of Br^- adducts of HOCl.

addition of bromoform to the corona discharge by bubbling N_2 through the liquid room temperature into the ion source produces peaks at $m/z = 131$, 133, and 135, corresponding to the formation of the adducts $Br^-{\cdot}HOCl$. The relative signal intensities are consistent with a compound containing one Br and one Cl (3:4:1). MS/MS product scans using $CHBr_3$ are very similar to the product scan of the analogous Cl^- species in ambient air, where the only masses observed are those of the bromide ion contributing to the adduct. The Br^- adduct of Cl_2O has also been observed in these studies and can be used to unambiguously identify such impurities.

Although the focus of these studies was on the characterization of the atmospheric pressure ionization mass spectrum of HOCl, rather than on its detection limits under atmospheric conditions, it is clear that API-MS is a powerful tool for studying HOCl chemistry under tropospheric conditions. Thus, comparison of the signal intensities we observed using EI-MS to those from API-MS shows that the latter is at least several orders of magnitude more sensitive for samples at 1 atm pressure.

Under our experimental conditions, the HOCl adduct peak intensities for 100 ppm of HOCl are on the same order of magnitude as those for 90 ppb Cl_2; i.e., similar peak intensities are obtained in the Q1 scan for HOCl concentrations which are $\sim 10^3$ times larger. Spicer et al.[20] have shown that Cl_2 can be measured in air using API-MS, with a detection limit of 16 ppt, suggesting that HOCl should be detectable at concentrations of ~16 ppb, which is useful in laboratory studies of HOCl reactions at atmospheric pressure. However, greatly improved sensitivity and specificity for the HOCl adducts can be obtained by adjustment of the ionization and CAD gas conditions and by use of MS/MS. For example, Spicer et al.[38] have measured HONO at 1 atm pressure by formation of the Cl^- adduct, with detection limits of ~0.5 ppb. It is expected that optimization of the analytical conditions would lead to similar detection limits for HOCl.

There are no field measurements of HOCl in the troposphere. Peak concentrations of HOCl in the marine boundary layer are predicted from modeling studies[16,17,20] to be in the range of a few to several hundred ppt, with the higher value based on model predictions using measurements of Cl_2 in the marine boundary layer.[20] It is therefore not clear whether API-MS will be sufficiently sensitive for the identification and quantification of HOCl under atmospheric conditions. Further studies directed to optimizing detection of HOCl in the presence of the other chlorine compounds found in air need to be carried out to address this issue.

Conclusions

API-MS has been shown to be a powerful technique for detecting gas-phase HOCl at atmospheric pressure. Though ionization at atmospheric pressure is readily and efficiently achieved with a corona discharge, molecular species can undergo a number of reaction processes to form ions, depending on the nature of the gases present. Hence, the spectrum produced is rather complex. Ion−neutral adduct formation, however, greatly facilitates identification of such species as HOCl and Cl_2O. In ambient air, HOCl and Cl_2O form adducts with Cl^- and OCl^- and, when bromoform is added to the source, with Br^-. HOCl also forms an adduct with O_2^-. Impurities such as Cl_2 and HCl are readily discernible since O_2^- generated in ambient air under the influence of the corona discharge undergoes charge transfer with Cl_2, producing Cl_2^-, and adduct formation with HCl, producing $O_2^-{\cdot}HCl$; in the presence of other chlorine atom sources, HCl also forms the $Cl^-{\cdot}HCl$ adduct. With optimization of the ionization and collisionally induced dissociation conditions, this approach may also prove useful for ambient air studies.

Acknowledgment. T.E.C. thanks the Camille and Henry Dreyfus Foundation for financial support as a Dreyfus Environmental Postdoctoral Research Fellow, and S.L. thanks the Knut and Alice Wallenberg Foundation for financial support during a visit to this laboratory. We also thank the Department of Energy and the National Science Foundation for support of this research, R. Atkinson and C. W. Spicer and colleagues for their detailed guidance and advice on API-MS, J. S. Francisco for calculation of the electron affinity of HOCl, and R. McIver and F. Fehsenfeld for helpful discussions.

References and Notes

(1) World Meterological Organization, "Scientific Assessment of Ozone Depletion: 1994", 1995.

(2) Brune, W. H., Stratospheric Chemistry-Perspectives in Environmental Chemistry In *Perspectives in Environmental Chemistry*; Macalady, D. L., Ed.; Oxford University Press: New York, 1998; Chapter 13, pp 292−324.

(3) Ennis, C. A.; Birks, J. W. *J. Phys. Chem.* **1985**, *89*, 186.

(4) Chu, L. T.; Leu, M.-T.; Keyser, L. F. *J. Phys. Chem.* **1993**, *97*, 12798.

(5) Zhang, R.; Leu, M.-T.; Keyser, L. F. *J. Phys. Chem.* **1994**, *98*, 13563.

(6) Abbatt, J. P. D.; Nowak, J. B. *J. Phys. Chem.* **1997**, *101*, 2131.
(7) Abbatt, J. P. D.; Molina, M. J. *Geophys. Res. Lett.* **1992**, *19*, 461.
(8) Oppliger, R.; Allanic, A.; Rossi, M. J. *J. Phys. Chem.* **1997**, *101*, 1903.
(9) Hanson, D. R.; Ravishankara, A. R. *J. Phys. Chem.* **1992**, *96*, 2682.
(10) Viggiano, A. A.; Arnold, F. *Planet. Space Sci.* **1981**, *29*, 895.
(11) McCrumb, J. L.; Arnold, F. *Nature* **1981**, *294*, 136.
(12) Schlager, H.; Arnold, F. *Planet. Space Sci.* **1987**, *35*, 693.
(13) Finlayson-Pitts, B. J. *Res. Chem. Intermed.* **1993**, *19*, 235.
(14) Keene, W. C. *Naturally-Produced Organohalogens*; Grimvall, A., Leer, E. W. B. d., Eds.; Kluwer Academic Publishers: NY, 1995.
(15) DeHaan, D. O.; Brauers, T.; Oum, K.; Stutz, J.; Nordmeyer, T.; Finlayson-Pitts, B. J.; et al. *Int. Rev. Phys. Chem.* **1999**, in press.
(16) Sander, R.; Crutzen, P. J. *J. Geophys. Res.* **1996**, *101*, 9121.
(17) Vogt, R.; Crutzen, P. J.; Sander, R. *Nature* **1996**, *383*, 327.
(18) Spicer, C. W.; Kenny, D. V.; Shaw, W. J.; Busness, K. M.; Chapman, E. G. *Environ. Sci. Technol.* **1994**, *28*, 412A.
(19) Kotasek, V. Masters Thesis, University of Toronto, 1981.
(20) Spicer, C. W.; Chapman, E. G.; Finlayson-Pitts, B. J.; Plastridge, R. A.; Hubbe, J. M.; Fast, J. M.; Berkowitz, C. M. *Nature* **1998**, *394*, 353.
(21) Schindler, R. N.; Liesner, M.; Schmidt, S.; Kirchner, U.; Benter, Th. *J. Photochem. Photobiol. A* **1997**, *107*, 9.
(22) Vogt, R.; Schindler, R. N. *Ber. Bunsen-Ges. Phys. Chem.* **1993**, *97*, 819.
(23) Francisco, J. S. personal communication.
(24) Lide, D. R. Ed. *Handbook of Chemistry and Physics*, CRCnetBase, 1999, Chapman and Hall: 1999.
(25) Lias, S. G.; Bartmess, J. E.; Liebman, J. F.; Holmes, J. L.; Levin, R. D.; Mallard, W. G. *J. Phys. Chem. Ref. Data* **1988**, *17*, Suppl. No. 1.
(26) Fehsenfeld, F. C.; Howard, C. J.; Schmeltekopf, A. L. *J. Chem. Phys.* **1975**, *63*, 2835.
(27) Mirri, A. M.; Scappini, F.; Cazzoli, G. *J. Mol. Spectrosc.* **1971**, *38*, 218.
(28) Rosen, B., *Tables Internationales de Constantes Selectionnees*; Pergamon, New York, 1970; Vol. 17.
(29) Spinks, J. W. T.; Woods, R. J. *An Introduction to Radiation Chemistry*; Wiley: New York, 1990.
(30) Fehsenfeld, F. C.; Ferguson, E. E. *J. Chem. Phys.* **1974**, *61*, 3181.
(31) Yamdagni, R.; Kebarle, P. *J. Am. Chem. Soc.* **1971**, *93*, 7139.
(32) Spears, K. G.; Ferguson, E. E. *J. Chem. Phys.* **1973**, *59*, 4174.
(33) Payzant, J. D.; Yamdagni, R.; Kebarle, P. *Can. J. Chem.* **1971**, *49*, 3308.
(34) Mebel, A. M.; Morokuma, K. *J. Phys. Chem.* **1996**, *100*, 2985.
(35) Francisco, J. S. *Chem. Phys. Lett.* **1996**, *260*, 485.
(36) Dzidic, I.; Carroll, D. I.; Stillwell, R. N.; Horning, E. C. *J. Am. Chem. Soc.* **1974**, *96*, 5258.
(37) Huey, L. G.; Hanson, D. R.; Howard, C. J. *J. Phys. Chem.* **1995**, *99*, 5001.
(38) Spicer, C. W.; Kenny, D. V.; Billick, I. H.; Ward, G. F. *J. Air Waste Manage. Assoc.* **1993**, *43*, 1479.